Packed red blood cells inhibit T-cell activation *via* ROS-dependent signaling pathways

Marlene C. Gerner[1,2] , Andrea Bileck[3,4] , Lukas Janker[3,4] , Liesa S. Ziegler[2], Thomas Öhlinger[5], Pierre Raeven[5], Ernst W. Müllner[6], Ulrich Salzer[6], Christopher Gerner[3,4] , Klaus G. Schmetterer[2,+] , and David M. Baron[5,*,+]

From the [1]Division of Biomedical Science, University of Applied Sciences FH Campus Wien, Vienna, Austria; [2]Department of Laboratory Medicine, Medical University of Vienna, Vienna, Austria; [3]Department of Analytical Chemistry, Faculty of Chemistry and [4]Joint Metabolome Facility, Faculty of Chemistry, University of Vienna, Vienna, Austria; and [5]Department of Anaesthesia, Intensive Care Medicine and Pain Medicine and [6]Center of Medical Biochemistry, Max Perutz Labs (MPL), Medical University of Vienna, Vienna, Austria

Edited by Peter Cresswell

Numerous observations indicate that red blood cells (RBCs) affect T-cell activation and proliferation. We have studied effects of packed RBCs (PRBCs) on T-cell receptor (TCR) signaling and the molecular mechanisms whereby (P)RBCs modulate T-cell activation. In line with previous reports, PRBCs attenuated the expression of T-cell activation markers CD25 and CD69 upon costimulation *via* CD3/CD28. In addition, T-cell proliferation and cytokine expression were markedly reduced when T-cells were stimulated in the presence of PRBCs. Inhibitory activity of PRBCs required direct cell–cell contact and intact PRBCs. The production of activation-induced cellular reactive oxygen species, which act as second messengers in T-cells, was completely abrogated to levels of unstimulated T-cells in the presence of PRBCs. Phosphorylation of the TCR-related zeta chain and thus proximal TCR signal transduction was unaffected by PRBCs, ruling out mechanisms based on secreted factors and steric interaction restrictions. In large part, downstream signaling events requiring reactive oxygen species for full functionality were affected, as confirmed by an untargeted MS-based phosphoproteomics approach. PRBCs inhibited T-cell activation more efficiently than treatment with 1 mM of the antioxidant *N*-acetyl cysteine. Taken together, our data imply that inflammation-related radical reactions are modulated by PRBCs. These immunomodulating effects may be responsible for clinical observations associated with transfusion of PRBCs.

Following specific T-cell receptor (TCR) stimulation in lymphoid organs, T-cells can transmigrate into tissues, primarily exerting their immunological functions in the interstitium. Numerous checkpoints and control mechanisms that interrupt T-cell activation prevent unspecific stimulation and harmful consequences such as autoimmune disease (1). Among numerous other factors, the quantity and quality of T-cell activation depends on the metabolic micromilieu (*i.e.*, availability of carbohydrates, lipids, or amino acids) and on local concentrations of small molecules, electrolytes, oxygen, and reactive oxygen species (ROS). Thus, the alteration of metabolism offers multiple targets for intervention of T-cell responses (2–4). In this context, T-cells may also serve as a model to improve our knowledge of cell activation, proliferation, apoptosis, and survival (5–7).

Previous observations indicate that red blood cells (RBCs) act as modulators of T-cell growth and survival (8, 9) and have been linked to enhanced T-cell proliferation (9, 10). These effects were in part mediated by RBC-derived factors (11). RBCs can be processed and stored as packed red blood cells (PRBCs) for up to 42 days before being transfused. During prolonged storage, PRBCs undergo biochemical changes. Research has shown that PRBCs can modulate the immune system of the recipient, which is referred to as transfusion-related immunomodulation. In particular, PRBCs suppressed T-cell proliferation *via* cell–cell contact in a dose-dependent manner (12) and decreased cytokine production in T-cells (13). Moreover, RBC-derived extracellular vesicles induced both inflammatory and immunosuppressive effects (14).

Similarly, conflicting results were reported in clinical studies of PRBC transfusion. Patients receiving intraoperative PRBCs had a higher risk to develop systemic inflammation (15). In line, extracellular vesicles from fresh and stored PRBCs may mediate a strong proinflammatory host response associated with an enhanced production of proinflammatory cytokines (16–18). Contrarily, in two other studies, PRBCs and hemolytic products of RBCs suppressed immune function *in vitro* and *in vivo* (19, 20). Some of these differences may relate to alterations of RBC metabolism during storage or to specific patient populations (21). Proteomics-based investigations have revealed alterations of RBC metabolism, depending on genetic background of donors and storage of PRBCs, which may further explain differences among studies (22, 23).

We have previously reported mechanisms involved in the regulation of T-cell function (6, 24–27), focusing on distinct signaling events and/or transcriptional signatures. In this respect, modulation of receptor-mediated signaling cascades of T-cells has been linked with radical stress management and cell metabolism (5). In the present investigation, we focused on

---

‡ These authors contributed equally to this work.
* For correspondence: David M. Baron, david.baron@meduniwien.ac.at.

a detailed analysis of the effects of PRBCs on T-cell activation using primary human cells.

Results

PRBCs inhibit activation and proliferation of CD4^{+} T-cells

To determine the inhibitory effect of PRBCs on CD4^{+} T-cells, CD4^{+} T-cells were activated during incubation with increasing numbers of PRBCs. Expression of the activation markers CD25 (interleukin-2 [IL-2] receptor alpha chain) and CD69 (transmembrane C-type lectin) was used as readouts for early T-cell activation, since these two molecules are upregulated within the first hours following TCR stimulation. These activation markers were markedly reduced on stimulated CD4^{+} T-cells in coculture with PRBCs starting at a PRBC:CD4^{+} T-cell ratio of 12:1 (Fig. 1, *A* and *B*). At PRBC:CD4^{+} T-cell ratios greater than 50:1, CD25 and CD69 expression did not differ from that observed at a ratio of 50:1. Thus, we used a PRBC:CD4^{+} T-cell ratio of 50:1 for subsequent experiments (Fig. 1*C*). The proliferation rate of stimulated CD4^{+} T-cells was reduced in coculture with PRBCs (Fig. 1*D*). Similarly, PRBCs reduced the mRNA expression of the T-cell growth factor IL-2 (Fig. S1*A*) and Th1-, Th2-, and Th17-related cytokines (Fig. S1, *B–D*) in stimulated CD4^{+} T-cells. Furthermore, coculture with PRBCs reduced activation-induced mRNA expression levels of the transcription factor MYC (Fig. S1*E*), which is involved in metabolic reprogramming of activated T-cells as well as in T-cell growth and proliferation (28). Monocytes, B-cells, or natural killer cells did not interfere with the inhibitory effect of PRBCs, as PRBCs in the presence of peripheral blood–derived mononuclear cells (PBMCs) also inhibited anti-CD3/anti-CD28 monoclonal antibody–mediated T-cell activation (Fig. S1*F*).

Next, we compared the inhibitory effect of PRBCs on naïve and memory T-cells, as these cell types differ in their metabolic and functional states. PRBCs inhibited the activation of both naïve and memory T-cells (Fig. S1*F*). Previous studies have shown that heme, a major compound of hemoglobin, is released during hemolysis (29). Heme has immunomodulatory properties and strongly inhibits phagocytosis and migration of phagocytes (19). Thus, we tested whether PRBC lysates containing heme or purified PRBC membranes would inhibit T-cell activation. In these experiments, only intact PRBCs were able to modulate activation-induced CD25 upregulation on T-cells (Figs. 1*E* and S2*A*) In addition, direct cell–to–cell contact of PRBCs and CD4^{+} T-cells was required, as the inhibitory effect was abolished when PRBCs and CD4^{+} T-cells were cocultured using transwell plates (Figs. 1*F* and S2*B*). Suppression of T-cell responses by PRBCs did not apparently induce Treg polarization or anergy since the expression of FOXP3 did not differ between stimulated CD4^{+} T cells incubated in the presence or the absence of PRBCs (Fig. 1*G*). Similarly, the anergy-associated factor p27kip1 (30) was not altered by coincubation with PRBCs (Fig. S2*C*).

As the next step, we tested the ability of PRBCs stored for different periods to inhibit CD4^{+} T-cell activation. Storage duration had a minor effect on the ability of PRBCs to inhibit CD25 expression on CD4^{+} T-cells (Fig. S3*A*). Activated CD4^{+} T-cells secreted more IL-2 as storage duration of cocultured PRBCs increased, but even PRBCs stored until the regulatory limit of 42 days significantly inhibited IL-2 secretion (Fig. S3*B*).

PRBCs inhibit T-cell activation–induced ROS generation and express high levels of enzymes regulating oxidation

ROS produced by mitochondria are known to act as a critical second messenger for T-cell receptor signaling and T-cell activation and directly coregulate IL-2 production (31). PRBCs modulate redox activity and provide antioxidative protection in their microenvironment but may also exert prooxidative activities in human disease (32). We therefore evaluated the influence of PRBCs on the oxidative potential of activated CD4^{+} T-cells. Activation-induced mitochondrial superoxide production was significantly reduced in the presence of PRBCs (Fig. 2*A*), which was corroborated by corresponding changes in mitochondrial membrane potential (Fig. 2*B*). Similarly, total cellular ROS generated during T-cell activation was inhibited to levels of unstimulated CD4^{+} T-cells by coincubation with PRBCs (Fig. 2*C*).

Proteomic analyses of PRBC identified 732 protein groups and indicate that redox proteins are highly expressed in PRBCs compared with CD4^{+} T-cells (Fig. 2*D* and Table S2). Accordingly, PRBC rapidly degraded hydrogen peroxide (H_2O_2) (Fig. 2*E*). The enzymatic inhibitor sodium azide (NaN_3) significantly slowed but did not completely inhibit degradation of H_2O_2 (Fig. 2*E*). To independently demonstrate the impact of redox modulation leading to CD4^{+} T-cell inhibition, we also performed activation assays in the presence of the antioxidant *N*-acetyl-L-cysteine (NAC) instead of PRBCs (Fig. S4, *A–C*). Both PRBCs and NAC reduced the number of CD25- and CD69-expressing CD4^{+} T-cells as well as the mRNA expression of IL-2 (Fig. S4, *A* and *B*, respectively). Phosphorylation of the TCR zeta chain (CD247) was increased following anti-CD3/anti-CD28–mediated TCR stimulation, an effect that was not modulated by PRBCs or NAC (Fig. S4*C*).

Phosphoproteomic profiling demonstrates suppression of mitogen-activated protein kinase, cyclin-dependent kinase 5, and mechanistic target of rapamycin kinases upon coincubation with PRBCs

Phosphoproteomic analyses of activated CD4^{+} T-cells in presence of PRBCs or NAC identified 2310 phosphopeptides corresponding to 691 phosphoprotein groups (Table S3). Mapping the differentially expressed phosphopeptides to kinase activities revealed key signaling events significantly triggered upon T-cell activation such as eight distinct MAP-kinases, mechanistic target of rapamycin (mTOR), cyclin-dependent kinase 5, ribosomal protein S6 kinase, among others (Fig. 3*A*). Interestingly, cell activation not only caused the activation of signaling cascades but also resulted in the significant suppression of kinase activities including three distinct casein kinases (Fig. 3*A*). Coincubation with PRBCs significantly reduced the kinase activities of five MAP kinases as well as cyclin-dependent kinase 5 and mTOR but apparently restored casein kinase activity (Fig. 3*B*). Treatment with NAC caused largely similar but less pronounced effects
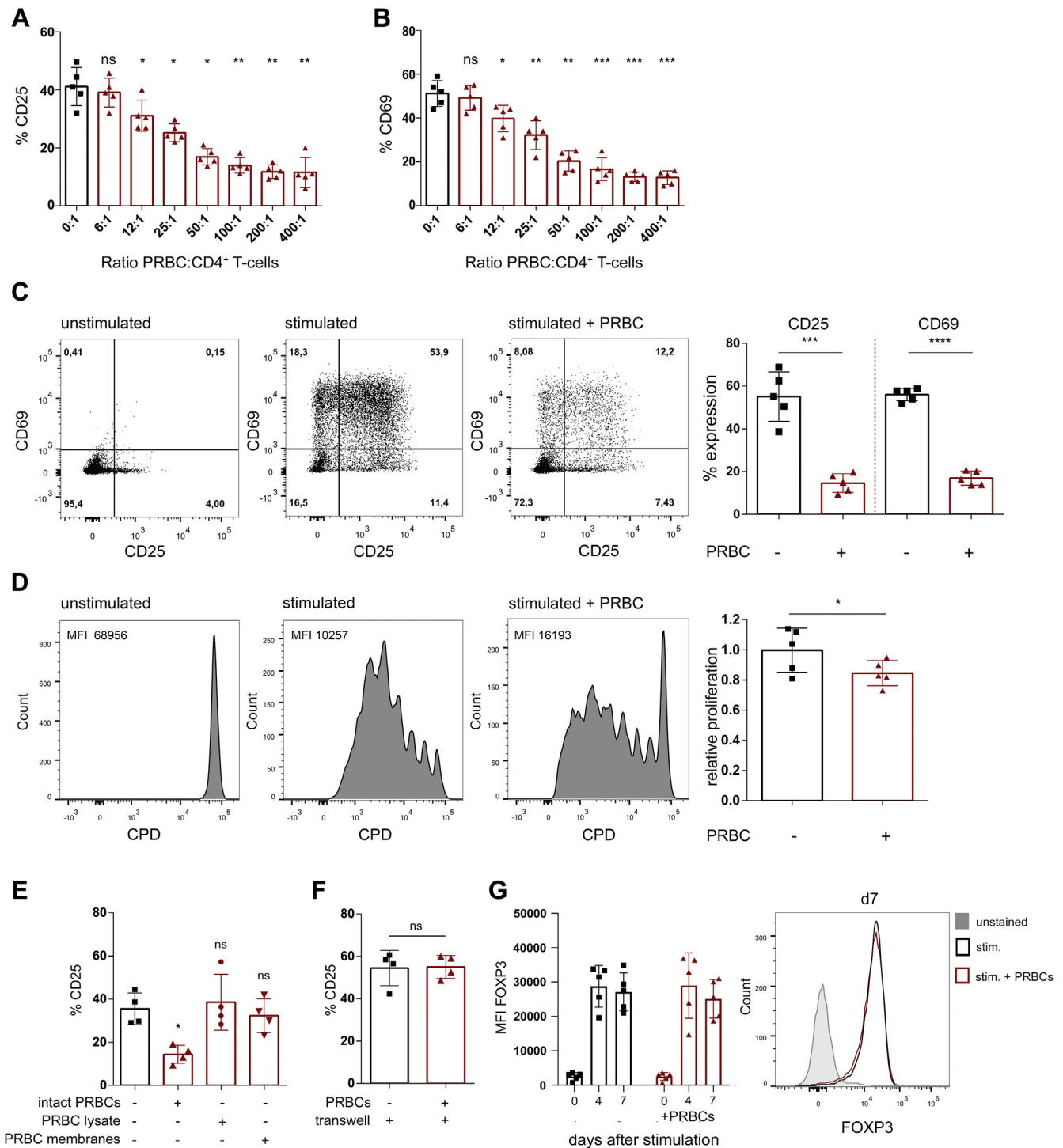
Figure 1. Activation of CD4+ T-cells is inhibited by the presence of packed red blood cells (PRBCs). *A* and *B*, CD4+ T-cells were activated in the presence of the indicated PRBC:CD4+ T-cell ratios. At 24 h after activation, CD25 (*A*) and CD69 (*B*) were measured by flow cytometric analysis. Data show percentage of CD25-/CD69-positive CD4+ T-cells normalized to unstimulated CD4+ T-cells and are presented as mean ± SD; ns, $p > 0.05$; *$p < 0.05$; **$p < 0.01$; ***$p < 0.001$ (one-way ANOVA). *C* and *D*, CD4+ T-cells were activated, and PRBCs were added at a ratio of 50:1 (PRBCs:T-cells). *C*, at 24 h after activation, the activation markers CD25 and CD69 were assessed by flow cytometric analysis. *Left*, fluorescence-activated cell sorting blots of one representative donor. *Right*, percentage of CD25-/CD69-positive cells in the presence/absence of PRBCs; values of unstimulated cells were subtracted. Data are presented as mean ± SD. ***$p < 0.001$; ****$p < 0.0001$ (paired *t* test). *D*, cell proliferation dye (CPD)-labeled CD4+ T-cells were activated in the presence/absence of PRBCs. Four days after stimulation, the proliferation rate of CD4+ T-cells was measured by flow cytometry. *Left*, histograms of one representative donor. Numbers indicate mean fluorescence intensity of CPD. *Right*, data are presented as proliferation index relative to stimulated cells in the absence of PRBCs. **$p < 0.01$ (paired *t* test). *E* and *F*, CD4+ T-cells were activated with anti-CD3/anti-CD28–coated microbeads in the presence of (*E*) intact PRBCs, PRBC lysate, or PRBC membrane fraction at a ratio of 50:1 (PRBCs:T-cells) or (*F*) in a transwell plate (5.0 μm pores) preventing direct contact of CD4+ T-cells and PRBCs. At 24 h after activation, the activation marker CD25, gated on CD4+ T-cells, was assessed by flow cytometric analysis. Data are represented as mean ± SD. *E*, ns > 0.05; *$p < 0.05$ (one-way ANOVA). *F*, ns > 0.05 (paired *t* test). *G*, CD4+ T-cells were activated with anti-CD3/anti-CD28–coated microbeads, and PRBCs were added at a ratio of 50:1 (PRBCs:T-cells). FOXP3 was measured by flow cytometric analysis in unstimulated cells (day 0) or after 4 or 7 days of stimulation. *Left*, data are presented as mean ± SD. *Right*, histogram overlays of one representative donor.
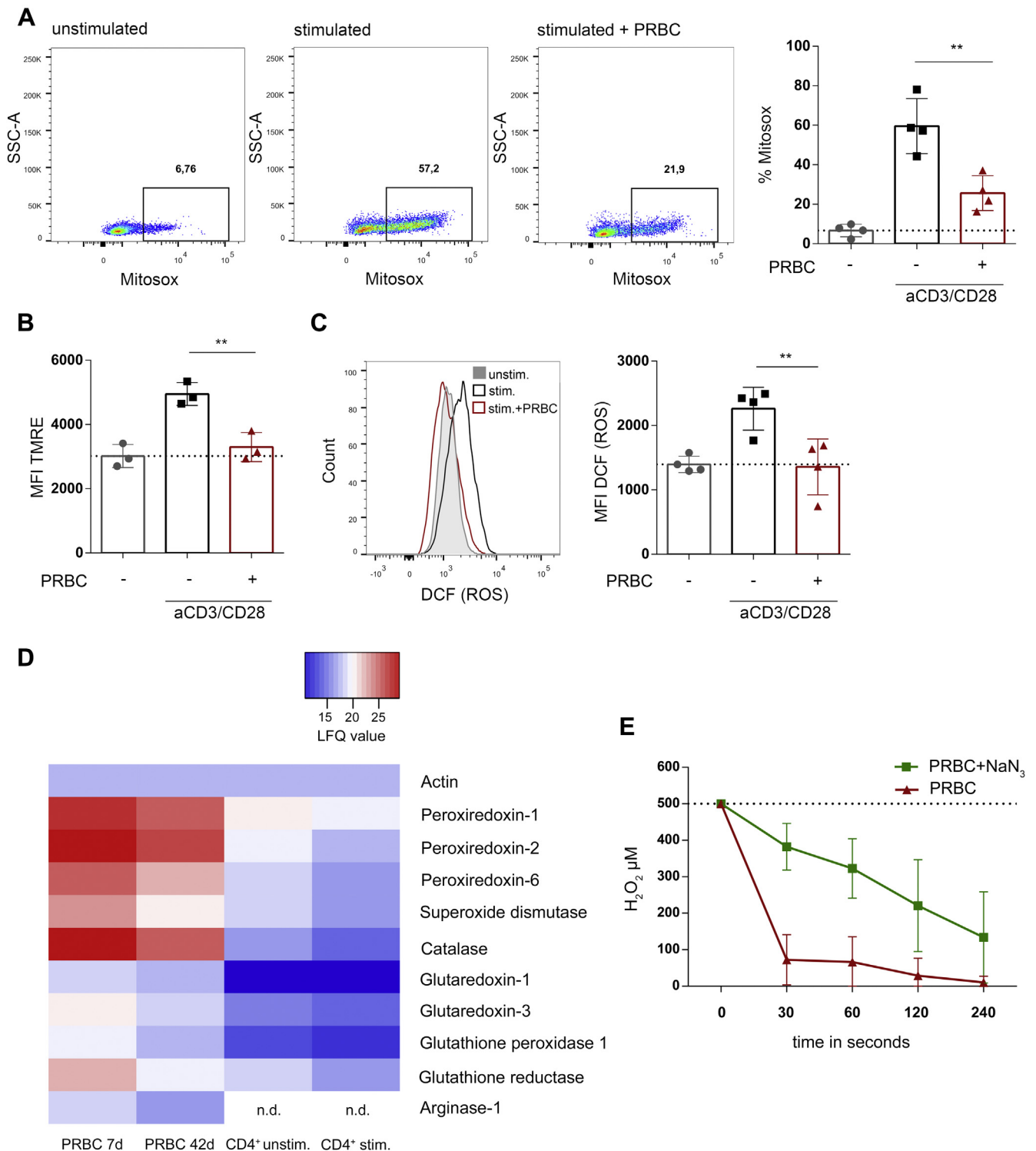
Figure 2. PRBCs) inhibit T-cell activation-induced reactive oxygen species (ROS) generation and express high levels of enzymes regulating oxidation. *A–C*, CD4^{+} T-cells were activated for 24 h with anti-CD3/anti-CD28–coated microbeads, and PRBCs were added in a ratio of 50:1 (PRBCs:T-cells). *A*, mitochondrial superoxide production was measured using the Mitosox dye. *Left*, fluorescence-activated cell sorting blots of one representative donor. Numbers above the gate indicate percentage of Mitosox-positive CD4^{+} T-cells. *Right*, statistical analyses. Data show percentage of Mitosox-positive CD4^{+} T-cells and are represented as mean ± SD; **$p < 0.01$ (paired *t* test). *B*, mitochondrial membrane potential was measured using the tetramethylrhodamine ethyl ester (TMRE) dye. Data show mean fluorescence intensity (MFI) of TMRE and are represented as mean ± SD. **$p < 0.01$ (paired *t* test). *C*, cellular ROS was measured using the 2′,7′-dichlorofluorescin (DCF) reagent. *Left*, fluorescence-activated cell sorting histogram overlays of one representative donor. *Right*, statistical analyses, data are represented as mean ± SD; **$p < 0.01$ (paired *t* test). *D*, for proteome analyses, PRBCs were analyzed after 7 and 42 days of storage. In addition, unstimulated CD4^{+} T-cells or CD4^{+} T-cells stimulated for 24 h were harvested, and proteome analyses were performed. The heat map shows log2 label-free quantification values, measuring relative protein abundance. Data were normalized to actin (n = 3). *E*, PRBCs were pretreated with PBS or PBS containing 150 μM sodium azide (NaN$_3$; for inhibition of redox proteins) and were then incubated with 500 μM hydrogen peroxide (H$_2$O$_2$) for indicated periods. H$_2$O$_2$ was measured in the supernatant using the Amplex Red H$_2$O$_2$ detection kit. Data are shown as mean ± SD (n = 4).
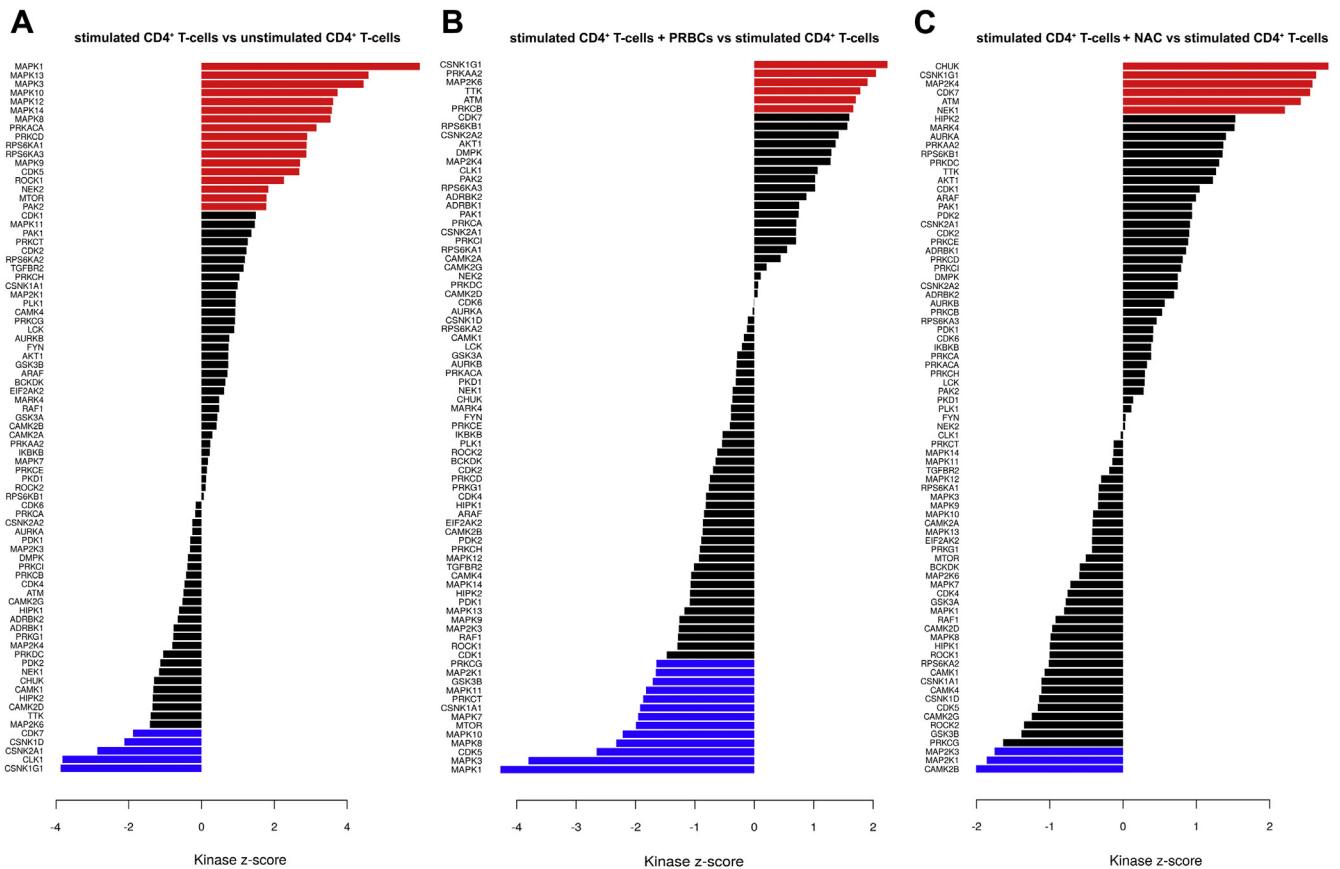
Figure 3. Kinase–substrate enrichment analysis of phosphoproteomic data of CD4^{+} T-cells stimulated in the the presence/absence of packed red blood cell (PRBC) (ratio of 50:1) or 1 mM *N*-acetyl-L-cysteine (NAC). Waterfall plots illustrating kinase–substrate enrichment analysis data for *A*, comparison of CD3-/CD28-stimulated CD4^{+} T-cells *versus* unstimulated-CD4^{+} T-cells (baseline; n = 5). *B*, comparison of CD3-/CD28-stimulated CD4^{+} T-cells coincubated with PRBCs *versus* CD3-/CD28-stimulated CD4^{+} T-cells (baseline; n = 5) and (*C*) comparison of CD3-/CD28-stimulated CD4^{+} T-cells coincubated with NAC *versus* CD3-/CD28-stimulated CD4^{+} T-cells (baseline; n = 5). Significantly altered kinase activities are illustrated by *red* or *blue*, for upregulation and downregulation, respectively. Significance thresholds were set to a NetworKIN score cutoff of 2, *p* value cutoff of 0.05, and substrate count cutoff of 5.

when compared with the effects of PRBCs (Fig. 3*C*). In order to illustrate to what extent the total kinome was affected by the treatments, kinome trees highlighting affected pathways are provided in Figures S5–S7 and Tables S4 and S5.

PRBCs selectively modulate downstream signaling in activated CD4^{+} T-cells

In parallel to the global phosphoproteomic profiling, selected major TCR downstream signaling nodes of T-cell activation were assessed using intracellular (IC) flow cytometry. During T-cell activation, one of the earliest events following anti-CD3/anti-CD28–mediated TCR stimulation is the phosphorylation of the TCR zeta chain (CD247). PRBCs did not interfere with CD247 phosphorylation (Fig. 4*A*) or phosphorylation of zeta chain–associated protein kinase 70 (Fig. S4*D*) at a PRBC:T-cell ratio of 50:1. Of note, phosphorylation of major downstream targets including S6 ribosomal protein (S6; a downstream target of the PI3K/Akt/mTOR pathway), p38, and NFkB were significantly reduced when CD4^{+} T-cells were activated in the presence of PRBCs (Fig. 4, *B–D*).

Discussion

In this study, we have confirmed that PRBCs inhibit T-cell activation. The observed effect was concentration dependent,

indicating a well-defined dose–response relationship and thus a mechanistic background.

The following experiments focused on the characterization of a molecular mechanism. In line with previous reports, the inhibitory effects were dependent on direct cell–cell contact rather than soluble factors. Phosphorylation of the TCR-associated zeta chain (CD247 pY142) was essentially unaffected by coincubation with PRBCs. Thus, we could rule out that binding of the stimulatory anti-CD3/anti-CD28 antibodies to their respective ligands was blocked by PRBCs. However, TCR downstream signaling events, such as phosphorylation of mTOR-related S6RP (pS240), p38 mitogen-activated protein kinase (pY182), and NFkB p65 (pS529), were inhibited by coincubation with PRBCs. Accordingly, we conclude that IC signaling events successfully initiated by stimulation of CD3/CD28 are blocked after initial signal transduction, and the main downstream targets were all inhibited.

T-cell signaling events propagate efficiently when phosphatase activities are inhibited by oxidative modifications of critical cysteine residues mediated by ROS. RBCs have previously been described to express a catalytic ring of proteins counteracting oxidative stress, required for their oxygen transport capability without causing exuberant oxidative damage (33). As a consequence, we suggest that the immune-
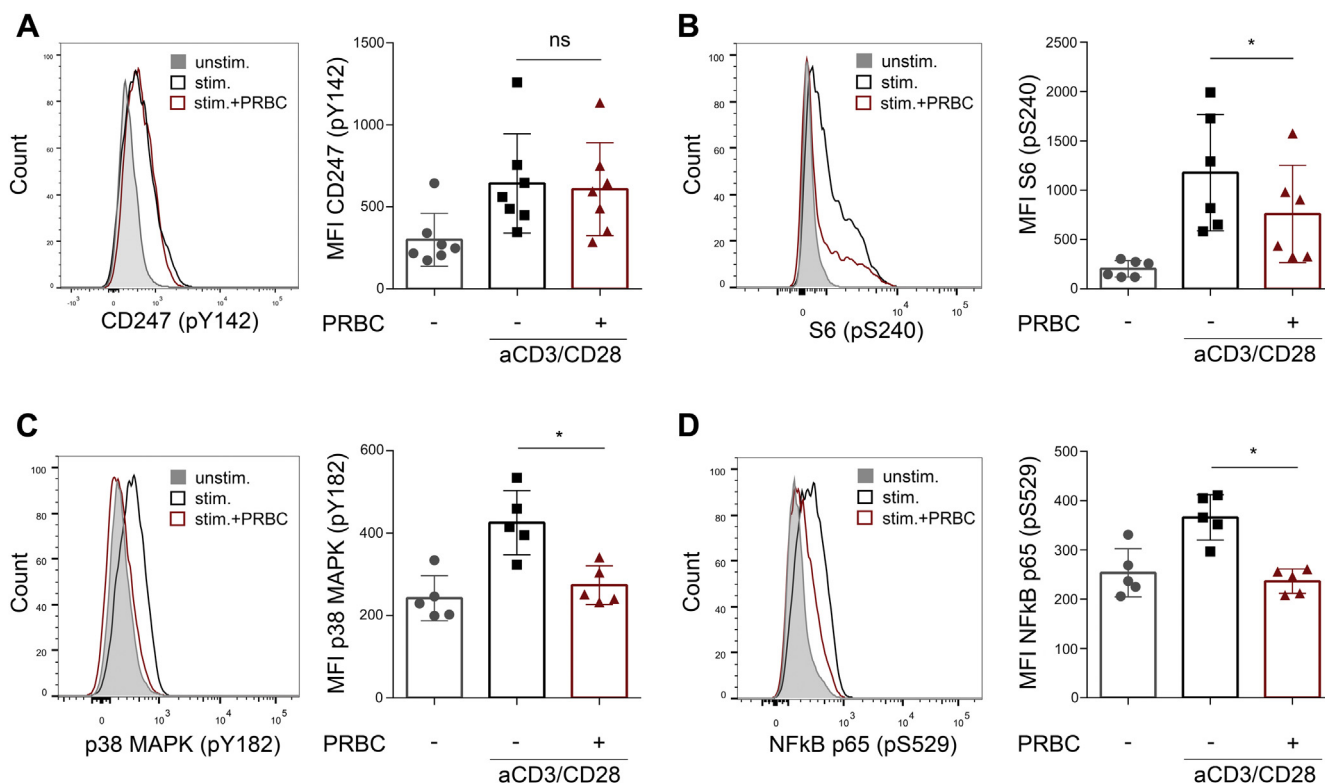
Figure 4. Upstream T-cell receptor (TCR) phosphorylation is fully activated, whereas downstream TCR signaling is inhibited by packed red blood cells (PRBCs) during CD4$^+$ T-cell activation. *A–D*, CD4$^+$ T-cells were activated with anti-CD3/anti-CD28, and PRBCs were added in a ratio of 50:1 (PRBCs:T-cells). *A*, at 1 h after activation, phosphorylation of the TCR-related zeta chain (CD247 pY142) was measured by flow cytometric analysis. *Left*, histogram overlays of one representative donor. *Right*, statistical analyses. Data are represented as mean ± SD. ns $p > 0.05$ (one-way ANOVA). At 24 h after activation, phosphorylation of the (*B*) mechanistic target of rapamycin–related S6RP (pS240), (*C*) p38 MAPK (pY183), and (*D*) NFkB p65 (pS529) was measured by fluorescence-activated cell sorting. *Left*, histogram overlays of one representative donor. *Right*, statistical analyses, mean fluorescence intensity (MFI) was set relative to unstimulated cells. Data are represented as mean ± SD. *$p < 0.05$ (one-way ANOVA).

modulatory effects of PRBCs on T-cells are based on their ability to prevent formation of critical ROS levels in neighboring T-cells required for successful amplification of signaling events. In line with this hypothesis, coincubation with PRBCs suppressed IC mitochondrial superoxide and total ROS formation in T-cells. Furthermore, treatment with the antioxidant NAC largely replicated the inhibitory effects of PRBCs. Support for these functional observations was also provided by an untargeted phosphoproteomics method, which independently verified the observations obtained with flow cytometric analysis. We again interpret this finding as a consequence of the H$_2$O$_2$ dissipation capacity of PRBCs.

The proposed model is fully compatible with and potentially explains all the apparently conflicting data reported and presented in previous studies. It is quite plausible that stressed old RBCs eventually release danger-associated molecular patterns mediating proinflammatory effects. These mechanisms are capable to trigger proinflammatory events, potentially by mainly acting as danger-associated molecular patterns on innate immune cells (34). Contrarily, direct cell–cell contact may mediate the anti-inflammatory and antiapoptotic effects repeatedly reported by attenuating formation of ROS. From a chemical perspective, H$_2$O$_2$ is known to act as a second messenger (35) capable of crossing cell membranes facilitated by aquaporins (36), which are known to be strongly expressed

by activated T-cells (37). RBC catalase, which dissipates H$_2$O$_2$, belongs to enzymes with the highest known turnover rates (38).

These considerations may have far-reaching consequences, which obviously require further investigation in the future. Inflammatory signaling involves radical reactions, which are crucial for oxidation of phosphatases and for the formation of inflammatory mediators (39). It is well recognized that inflammatory processes largely occur in the interstitium rather than full blood. Thus, RBCs may act as physiological buffers preventing inappropriate activation of T-cells during their migration phase from secondary lymphoid organs to the sites of inflammation. Once transmigrated to the interstitium free of RBCs, T-cells regain their full activation capacity and are therefore able to perform their effector functions. Thus, RBCs may also serve an important role in immune homeostasis. In this respect, especially solid tumors often present with increased RBC infiltration because of disorganized and inappropriate angiogenesis, which may support several features of tumorigenesis including deregulation of cellular energetics and avoiding immune destruction. T-cells are pivotal players in antitumor immunity and have high potency to even remove ongoing malignant processes. Given that many solid tumors display a high degree of vascular permeability due to disorganized angiogenesis, assessing the interaction between RBCs and T-cells may also impact future oncologic immunotherapies.

In conclusion, we present a mechanistic model explaining how (P)RBCs might modulate immune functions, especially T-cell activation. This model has potential implications on pathomechanisms such as vessel leakiness in solid tumors and the resulting inhibition of anticancer immune functions. We suggest that radical reaction products may be detectable in interstitial fluids rather than full blood, potentially serving as inflammatory *in situ* biomarkers. The described findings might promote future studies highlighting the physiological consequences of RBC/T-cell interactions.

Experimental procedures

Cells and cell culture

The study was approved by the local Ethics Committee of the Medical University of Vienna (protocol number: EK1043/2015) and registered at clinicaltrials.gov (NCT02639780). All experimental procedures were carried out in accordance with the ethical standards laid down in the Declaration of Helsinki. Peripheral blood buffy coat samples of healthy donors were provided by the Austrian Red Cross (Vienna, Austria) upon written informed consent. PBMCs were isolated by standard Ficoll–Paque centrifugation. $CD4^+$ T-cells were isolated using a MagniSort Human CD4 T-cell Enrichment Kit (Thermo Fisher Scientific) according to the manufacturing instructions. Purity assessed by flow cytometry was above 95% for $CD4^+$ T-cells. All functional assays were performed in Iscove's modified Dulbecco's medium (Gibco/Thermo Fisher Scientific) supplemented with 10% fetal calf serum (FCS; Gibco), 10 μg/ml gentamycin (Gibco), and 1.25 μg/ml amphotericin B (Lonza). RBCs were donated by healthy volunteers upon written informed consent. Demographic data of this donor cohort have been previously published (40). In short, blood was leukofiltered (log 4 leukocyte reduction), processed according to standard protocols of transfusion services of the Austrian Red Cross, and stored in a saline–adenine–glucose–mannitol solution under standard blood banking conditions at 4 °C for up to 42 days.

Fluorescence-activated cell sorting

For cell sorting, isolated $CD4^+$ T-cells were washed in PBS/0.5% FCS/2 mM EDTA (Sigma–Aldrich) and stained with antihuman mononuclear mouse antibodies against CD4 (clone OKT4, FITC conjugated) and CD45RO (clone UCHL1, APC-Cy7 conjugated; both Invitrogen). Cells were incubated at 4 °C for 30 min and washed thereafter. The technique to purify naïve and memory $CD4^+$ T-cells was fluorescence-activated cell sorting (FACS) sorted on a FACSAria Fusion cell sorter (BD Biosciences). Naïve $CD4^+$ T-cells were identified by the $CD4^+CD45RO^-$ phenotype and memory T-cells by the $CD4^+CD45RO^+$ phenotype. Purity assessed by flow cytometry was above 98%.

Stimulation of primary $CD4^+$ T-cells

$CD4^+$ T-cells were cultured with PRBCs at a ratio of 200:1 (PRBCs:PBMCs) or a ratio of 50:1 (PRBCs:$CD4^+$ T-cells). T-cells were activated with anti-CD3/anti-CD28–coated microbeads (Invitrogen; cells-to-beads ratio of 2:1). As control, $CD4^+$ T-cells were activated in the absence of PRBCs. All experiments were performed in either 12-well plates with 2×10^6 cells, 48-well plates with 3×10^5 cells, or 96-well plates with 1×10^5 cells. In some experiments, the antioxidant NAC (Sigma–Aldrich) was added to $CD4^+$ T-cells at a concentration of 1 mM.

Expression of $CD4^+$ T-cell activation markers

After 24 h in culture, cells were washed in PBS/0.5% FCS/0.05% NaN_3 (Sigma–Aldrich). Cells were incubated with anti-human mononuclear antibodies CD4 (clone SK3, phycoerythrin [PE]–Cyanine5.5 conjugated), CD25 (clone 2A3, PE conjugated), and CD69 (clone FN50, eFluor450 conjugated; all eBioscience) at RT for 15 min. PRBCs were lysed with BD FACS lysing solution for 10 min and washed with PBS/0.5% FCS/0.05% NaN_3. Cells were analyzed on a BD FACS Canto II flow cytometer and analyzed using the FlowJo software (version 10; BD Biosciences).

FOXP3 staining

$CD4^+$ T-cells were cultured in the presence/the absence of PRBCs at a ratio of 50:1 (PRBCs:$CD4^+$ T-cells) as indicated. PRBCs were lysed with BD FACS lysing solution for 10 min, and T-cells were stained with antihuman mononuclear antibodies against CD4 (clone SK3, PE–Cyanine5.5 conjugated) and prepared for IC staining using the eBioscience Foxp3/Transcription Factor Staining Buffer Set (Invitrogen) according to the manufacturer's recommendations. Cells were incubated with antihuman mononuclear antibody against FOXP3 (clone FJK-16s, PE–Cyanine7 conjugated; eBioscience) for 30 min at RT and washed with PBS/0.5% FCS/0.05% NaN_3. Cells were analyzed on a CytoFLEX (Beckman Coulter) flow cytometer and analyzed using the Kaluza Analysis software (Beckman Coulter).

p27 Kip1 staining

$CD4^+$ T-cells were cultured in the presence/absence of PRBCs at a ratio of 50:1 (PRBCs:$CD4^+$ T-cells), as indicated. PRBCs were lysed with BD FACS lysing solution for 10 min and were stained with antihuman mononuclear antibodies against CD4 (clone SK3, PE–Cyanine5.5 conjugated) followed by incubation in the IC fixation buffer (eBioscience) for 30 min at +4 °C. Cells were washed in PBS/0.5% FCS/0.05% NaN_3 and blocked with 2% bovine serum albumin/PBS for 30 min at RT. Cells were washed in 1× permeabilization buffer (eBioscience) and incubated with antihuman monoclonal antibody against p27 Kip1 (clone DCS-72.F6; Invitrogen) for 60 min at RT. Cells were washed in PBS/0.5% FCS/0.05% NaN_3 and were stained with Goat anti-Mouse IgG (H+L) Cross-Adsorbed Secondary Antibody (Alexa Fluor 488 conjugated; Invitrogen) for 40 min at RT. After washing, cells were resuspended in PBS/0.5% FCS/0.05% sodium azide and were analyzed on a CytoFLEX (Beckman Coulter) flow cytometer and analyzed using the Kaluza Analysis software.

Proliferation assay

$CD4^+$ T-cells were labelled with a cell-proliferationdye (CPD; eFluor 670; eBioscience) and were activated in the presence/

absence of PRBCs for 96 h. PRBCs were lysed with BD FACS lysing solution for 10 min, and proliferation was measured by flow cytometry. Proliferation rate was calculated using the following formula: *Division index = log (mean fluorescence unstimulated cells/mean fluorescence stimulated cells)/log (2)* (41).

Experiments using PRBC lysates, PRBC membranes, and transmembrane assay

PRBCs were lysed with water for 10 min at RT and centrifuged at $14,000g$ for 5 min. The PRBC lysate was supplemented with PBS, and the PRBC pellet containing PRBC membranes was washed twice with PBS. The used volume of lysate/membranes was adjusted to the amount of viable PRBCs. To test whether direct PRBC-CD4$^+$ T-cell contact is necessary to inhibit CD4$^+$ T-cell activation, PRBCs were added onto the bottom of a Costar transwell plate (Corning, Inc). CD4$^+$ T-cells were added onto a polycarbonate membrane with 5 μm pores, preventing a direct cell–cell contact between CD4$^+$ T-cells and PRBCs. CD4$^+$ T-cells were activated for the indicated time points, and mRNA expression of IL-2 or expression of the T-cell activation markers CD25 and CD69 was measured.

Quantitative PCR

About 4 h after T-cell activation, RNA was isolated using the RNeasy Mini Kit (Qiagen) according to the manufacturer's recommendations. Complementary DNA was generated by random hexamer-primed reverse transcription. Relative transcriptional levels of the indicated genes were quantified using the Luna Universal qPCR Master Mix (New England Biolabs) on a 7900HT Fast Real-Time PCR system (Applied Biosystems). Transcriptional levels of GAPDH were used as reference. Primers are listed in Table S1.

IL-2 ELISA

For quantitative detection of IL-2, IL-2 Human Uncoated ELISA Kit (Thermo Fisher Scientific) was used. Supernatants of cells were collected 24 h after activation and were diluted in a ratio of 1:5. The ELISA was performed according to the manufacturer's recommendations, and the plate was read at 450 nm (including wavelength subtraction of 570 nm from 450 nm).

Cellular ROS detection

For ROS detection, the 2′,7′-dichlorofluorescin diacetate (DCFDA) Cellular ROS Detection Assay Kit (Abcam) was used. In this assay, DCFDA, a fluorogenic dye, is deacetylated by cellular esterases and later oxidized by ROS into 2′,7′-dichlorofluorescein, a highly fluorescent compound that correlates with IC ROS activity and can be detected in the FITC channel. First, CD4$^+$ T-cells were labeled with a CPD (eFluor 670; eBioscience) to differentiate CD4$^+$ T-cells from PRBCs. At 24 h after T-cell activation in the presence/absence of PRBCs, 1 &times 10^5 cells were stained in culture medium with 20 μM DCFDA for 30 min at 37 °C and were then immediately transferred onto ice. Without washing, ROS levels on eFluor670-gated lymphocytes were quantified by flow cytometry in the FITC channel.

Mitosox assay

For detection of mitochondrial superoxide, the MitoSOX Red Mitochondrial Superoxide Indicator (Molecular Probes, Invitrogen) was used according to the manufacturer's recommendations. In this assay, MitoSOX Red reagent selectively targets mitochondria and is rapidly oxidized by superoxide but not by other ROS or reactive nitrogen species, yielding a red fluorescent compound. First, CD4$^+$ T-cells were labeled with a CPD (eFluor 670; eBioscience) to differentiate CD4$^+$ T-cells from PRBCs. At 24 h after CD4$^+$ T-cell activation in the presence/absence of PRBCs, 1 × 10^5 cells were washed and then stained in cell sort buffer containing PBS/0.5% FCS/2 mM EDTA with 5 μM MitoSOX Red reagent for 10 min at 37 °C and were then washed three times with cell sort buffer at RT. The expression of MitoSOX Red reagent was quantified on eFluor670-gated lymphocytes in the PE channel *via* flow cytometry.

Mitochondrial membrane potential

For the quantification of changes in mitochondrial membrane potential, the tetramethylrhodamine ethyl ester (TMRE)-Mitochondrial Membrane Potential Assay Kit (Abcam) was used. TMRE is a positively charged dye that accumulates in active mitochondria because of their relative negative charge. First, CD4$^+$ T-cells were labeled with a CPD (eFluor 670; eBioscience) to differentiate CD4$^+$ T-cells from PRBCs. Twenty-four hours after T-cell activation in the presence/absence of PRBCs, 1 × 10^5 cells were incubated with 50 nM TMRE for 30 min at 37 °C. Without washing, cells were analyzed *via* flow cytometry, and TMRE signal was detected in the PE channel.

H$_2$O$_2$ assay

To measure the capacity of PRBCs to degrade H$_2$O$_2$, 5 × 10^6 PRBCs were incubated in PBS in the presence of 500 μM H$_2$O$_2$ (Merck, Calbiochem) at indicated time points (30–240 s). Immediately after incubation, PRBCs were removed by centrifugation, and H$_2$O$_2$ concentration was measured in the supernatant using an Amplex Red Hydrogen Peroxide/Peroxidase Assay Kit (Invitrogen) according to the manufacturer's instructions. Absorbance was measured on a microplate reader at 560 nm. For inhibition of redox proteins including catalase, PRBCs were pretreated with 150 μM NaN$_3$ (Sigma–Aldrich) for 1 h at 37 °C and washed before testing H$_2$O$_2$ degradation.

IC phosphoprotein detection by flow cytometry

To determine whether phosphorylation of upstream or downstream targets of TCR signaling is inhibited by PRBCs, CD4$^+$ T-cells were activated in the presence/absence of PRBCs with plate-bound anti-CD3 and anti-CD28 for the indicated time points. PRBCs were then lysed on ice with BD FACS lysing solution for 10 min, and cells were fixed with BD Fixation buffer at 37 °C for 10 min. The fixation buffer was removed by centrifugation. The cell pellet was resuspended

with precooled 90% methanol and was incubated at –80 °C for 30 min to permeabilize the cell membranes. Afterward, the cells were washed twice with PBS/0.5% FCS/0.05% NaN$_3$. Cells were stained with following antihuman monoclonal antibodies: phospho-zeta chain (anti-CD247, pY142, clone K25-407.69, Alexa Fluor 647 conjugated; BD Phosflow), phospho-S6 (anti-pS240, clone N4-41, Alexa Fluor 647 conjugated; BD Phosflow), phospho-p38 (anti-p38 mitogen-activated protein kinase, pT180/pY182, clone 36/p38, PerCP Cy5.5. conjugated; BD Phosflow), or phospho-NFkB (anti-NFkB p65, pS529, clone K10-895.12.50, Alexa Fluor 488 conjugated; BD Phosflow) for 1 h at RT. Expression of phosphorylation status of the indicated targets was measured by flow cytometry.

Proteomics

PRBCs stored for 7 days or 42 days were washed and lysed using sample buffer (7.5 M urea, 1.5 M thiourea, 4% CHAPS, 0.05% SDS, and 100 mM DTT) and ultrasound after 7 and 42 days of storage. Protein concentration of PRBC lysates was determined *via* Bradford assay (Bio-Rad Laboratories). About 20 µg of protein from each sample were enzymatically digested using an adaption of the filter-aided sample preparation protocol as described previously (42, 43). Briefly, samples were preconcentrated onto prewashed 3 kDa molecular weight cutoff filters (Pall Austria Filter GmbH) by centrifugation at 15,000g for 15 min to obtain a final sample volume of 10 to 20 µl. Proteins were reduced and carbamidomethylated using DTT (5 mg/ml dissolved in 8 M guanidinium hydrochloride in 50 mM ammonium bicarbonate buffer; pH 8) and iodacetamide (10 mg/ml in 8 M guanidinium hydrochloride in 50 mM ammonium bicarbonate buffer), respectively. Afterward, 1 µg trypsin was added, and samples were incubated overnight at 37 °C. Peptide samples were further cleaned up using C-18 spin columns (Pierce, Thermo Scientific). Samples were dried and stored at –20 °C until further MS analyses.

For LC–MS/MS analysis, dried peptide samples were dissolved in 5 µl of 30% formic acid (FA) containing four synthetic standard peptides each 10 fmol/µl and further diluted with 40 µl mobile phase A (97.9% H$_2$O, 2% acetonitrile [ACN], and 0.1% FA), as described previously (43, 44). LC–MS/MS analyses were performed on a Dionex Ultimate 3000 nano LC system coupled to a QExactive orbitrap mass spectrometer, which was equipped with a nanospray ion source (Thermo Fisher Scientific). Each sample was analyzed in technical duplicates. A preconcentration of 5 µl of the peptide solution on a 2 cm × 75 µm C18 Pepmap100 precolumn (Thermo Fisher Scientific) was performed at a flow rate of 10 µl/min using mobile phase A. Afterward, peptides were eluted from the precolumn to a 50 cm × 75 µm Pepmap100 analytical column (Thermo Fisher Scientific) at a flow rate of 300 nl/min, and chromatographic separation was achieved applying a gradient from 7% to 40% mobile phase B (79.9% ACN, 20% H$_2$O, and 0.1% FA) over 41 min and a total LC run time of 85 min. Mass spectrometric detection was performed achieving MS scans in the range from m/z 400 to 1400 at a resolution of 70,000 (at m/z = 200). By applying higher energy collisional dissociation

fragmentation at 30% normalized collision energy, MS/MS scans of the eight most abundant ions were achieved and subsequently analyzed in the orbitrap at a resolution of 17,500 (at m/z =200).

Protein identification as well as label-free quantification was carried out using MaxQuant 1.5.2.8 (freeware © Max-Planck-Institute of Biochemistry) running Andromeda as search engine and searching against the SwissProt Database (version 201014 with 20,195 entries) (45). An allowed peptide tolerance of 25 ppm and a maximum of two missed cleavages were applied as search criteria. Furthermore, carbamidomethylation on cysteines was set as fixed modification, whereas methionine oxidation as well as N-terminal protein acetylation was set as variable modifications. In addition, a minimum of two peptide identifications per protein, at least one of them unique, was used as further search criteria. A 5 min match time window and a 15 min alignment time window were applied for achieving match between runs. All peptide as well as protein identifications were meeting a false discovery rate ≤0.01. After protein identification, proteins were filtered for common contaminants as well as reversed sequences, and data evaluation was performed using Perseus software (freeware © Max-Planck-Institute of Biochemistry; version 1.5.1.6) (46).

Proteomics data of unstimulated and stimulated CD4$^+$ T-cells have been previously published (6). To compare relative amounts of redox protein expression in PRBCs and CD4$^+$ T-cells, label-free quantification values were normalized to actin, ACTA1 (UniProtKB-P68133). The heat map was designed using heatmapper tool (http://www.heatmapper.ca/) (47).

Phosphoproteomics

About $1 × 10^7$ CD4$^+$ T-cells of five healthy donors were stimulated with CD3-/CD28-coated microbeads for 3 h in the presence/absence of PRBCs or 1 mM NAC. Thereafter, cells were washed thoroughly using RBC lysis buffer (154 mM NH$_4$Cl, 10 mM KHCO$_3$, and 100 µM Na$_2$ EDTA). Washed CD4$^+$ T-cells were lysed in lysis buffer (4% sodium deoxycholate, 100 mM Tris–HCl pH 8.5) followed by mechanical shear stress *via* ultrasonication and subsequent heat inactivation at 95 °C for 5 min.

For the posphopeptide enrichment, a modified protocol of the EasyPhos workflow was applied (48). Briefly, the total protein content of $1 × 10^7$ CD4$^+$ T-cells was used for the enrichment procedure. Protein reduction using 100 mM Tris-(2-carboxyethyl) phosphine and alkylation using 400 mM 2-carboxyamidomethylcysteine with subsequent enzymatic digestion with trypsin/Lys-C mixture (1:100 enzyme to substrate ratio) at 37 °C for 18 h was performed. The solution containing the peptides was mixed with enrichment buffer containing 48% TFA (v/v) and 8 mM potassium dihydrogen phosphate. Samples were incubated with 3 mg titanium dioxide Titansphere beads for 5 min at 40 °C with subsequent washing and elution from StageTips with 40% ACN and 5% ammonium hydroxide solution. Samples were dried and reconstituted in 15 µl MS loading buffer containing 97.7% H$_2$O, 2% ACN, and 0.3% TFA.

LC–MS/MS analysis was performed as described previously (49). In short, peptides were separated and detected using a Dionex Ultimate 3000 nano LC system (Thermo Fisher Scientific) coupled to a trapped ion mobility spectrometry time-of-flight Pro mass spectrometer (Bruker Daltonics). About 10 µl of phosphopeptide-enriched proteome samples were loaded on a 2 cm × 100 µm C18 Pepmap100 precolumn (Thermo Fisher Scientific) at a flow rate of 10 µl/min using mobile phase A. Afterward, peptides were eluted from the precolumn to a 25 cm × 75 µm 25 cm Aurora Series emitter column (IonOpticks) at a flow rate of 300 nl/min. Separation was achieved using a gradient of 8% to 40% mobile phase B (79.9% ACN, 20% H_2O, and 0.1% FA) over 90 min. The trapped ion mobility spectrometry time-of-flight Pro mass spectrometer was operated in the parallel accumulation serial fragmentation mode. Trapped ion mobility separation was achieved by applying a 1/k0 scan range from 0.60 to 1.60 V s/cm^2 resulting in a ramp time of 100 ms. All experiments were performed with ten parallel accumulation serial fragmentation MS/MS scans per cycle leading to a total cycle time of 1.16 s. MS and MS/MS spectra were recorded using a scan range (m/z) from 100 to 1700. Further, the collision energy was ramped as a function of increasing ion mobility from 20 to 59 eV, and the quadrupole isolation width was set to 2 Th for $m/z < 700$ and 3 Th for $m/z > 800$. For each experimental group, five biological replicates were obtained. All samples were measured once, resulting in a total number of 20 measurements.

Data analysis was performed using MaxQuant 1.6.17.0 (45) employing the Andromeda search engine for protein identification against the UniProt Database (version 12/2019 with 20,380 entries) allowing a mass tolerance of 20 ppm for MS spectra and 40 ppm for MS/MS spectra, a false discovery rate of <0.01, and a maximum of two missed cleavages. Furthermore, search criteria included carbamidomethylation of cysteine as fixed modification and methionine oxidation, N-terminal protein acetylation, as well as phosphorylation of serine, threonine, and tyrosine as variable modifications.

For the evaluation of phosphoproteomics data, a two-sided t test of site-centric intensity values between experimental groups was performed, with subsequent kinase–substrate enrichment analysis of class 1 phosphosites ($p > 0.75$) utilizing PhosphoSitePlus and NetworKIN, applying a NetworKIN score cutoff of 2, p value cutoff of 0.05, and substrate count cutoff of 5 (50–52). For the visualization of enriched kinases in context of the global kinome, the Coral application (freeware © 2018 Phanstiel Lab) was used (53).

Western blot

About 1×10^7 CD4$^+$ T-cells were stimulated with aCD3-/CD28-coated microbeads for 30 min in the presence/absence of PRBCs or 1 mM NAC. Thereafter, cells were washed thoroughly using RBC lysis buffer (154 mM NH$_4$Cl, 10 mM KHCO$_3$, and 100 µM Na$_2$ EDTA). Washed CD4$^+$ T-cells were lysed with radioimmunoprecipitation assay buffer supplemented with protease inhibitor and phosphatase inhibitors (all Sigma–Aldrich). After 30 min of incubation on ice with periodic pulse vortexing, cell lysates were centrifuged at 16,000g for 15 min at +4 °C. For equal loading, protein concentration was measured using Pierce BCA Protein Assay Kit (Thermo Fisher Scientific) according to manufacturing instructions. A 4%–12% SDS-PAGE (Bio-Rad) was used to separate proteins following a transfer onto polyvinylidene difluoride membranes (GE Healthcare). The membrane was blocked with bovine serum albumin (Sigma–Aldrich), and the following antibodies were used for incubation overnight: Phospho-Zap-70 (Tyr319)/Syk (Tyr352) (1:2000, #2701; Cell Signaling Technology) and total Zap-70 (1:1000, 99F2; Cell Signaling Technology). Protein bands were visualized using horseradish peroxidase–linked anti-rabbit (Cell Signaling Technology) or antigoat (Abcam) antibodies and SuperSignal West Pico Chemiluminescent Substrate (Thermo Fisher Scientific).

Data availability

All data are contained within the article and the supporting information. Proteomic data of CD4$^+$ T-cells (Fig. 2D) have been previously published (6).

The MS proteomics data have been deposited to the ProteomeXchange Consortium (http://proteomecentral.proteomexchange.org) *via* the PRIDE partner repository (54) with the data set identifier PXD023144.

Annotated spectra from the phosphoproteomics data set were uploaded to the MS-Viewer repository (55). Data can be accessed with the unique search key 64ofijyrob.

References

1. Guram, K., Kim, S. S., Wu, V., Sanders, P. D., Patel, S., Schoenberger, S. P., Cohen, E. E. W., Chen, S.-Y., and Sharabi, A. B. (2019) A threshold model for T-cell activation in the era of checkpoint blockade immunotherapy. *Front. Immunol.* **10**, 491

2. Chapman, N. M., Boothby, M. R., and Chi, H. (2020) Metabolic coordination of T cell quiescence and activation. *Nat. Rev. Immunol.* **20**, 55–70

3. Shyer, J. A., Flavell, R. A., and Bailis, W. (2020) Metabolic signaling in T cells. *Cell Res.* **30**, 649–659

4. Le Bourgeois, T., Strauss, L., Aksoylar, H.-I., Daneshmandi, S., Seth, P., Patsoukis, N., and Boussiotis, V. A. (2018) Targeting T cell metabolism for improvement of cancer immunotherapy. *Front. Oncol.* **8**, 237

5. Franchina, D. G., Dostert, C., and Brenner, D. (2018) Reactive oxygen species: Involvement in T cell signaling and metabolism. *Trends Immunol.* **39**, 489–502

6. Gerner, M. C., Niederstaetter, L., Ziegler, L., Bileck, A., Slany, A., Janker, L., Schmidt, R. L. J., Gerner, C., Del Favero, G., and Schmetterer, K. G. (2019) Proteome analysis reveals distinct mitochondrial functions linked to interferon response patterns in activated CD4+ and CD8+ T cells. *Front. Pharmacol.* **10**, 727

7. Klein Geltink, R. I., O'Sullivan, D., Corrado, M., Bremser, A., Buck, M. D., Buescher, J. M., Firat, E., Zhu, X., Niedermann, G., Caputa, G., Kelly, B., Warthorst, U., Rensing-Ehl, A., Kyle, R. L., Vandersarren, L., *et al.* (2017) Mitochondrial priming by CD28. *Cell* **171**, 385–397

8. Fonseca, A. M., Porto, G., Uchida, K., and Arosa, F. A. (2001) Red blood cells inhibit activation-induced cell death and oxidative stress in human peripheral blood T lymphocytes. *Blood* **97**, 3152–3160

9. Arosa, F., Pereira, C., and Fonseca, A. (2004) Red blood cells as modulators of T cell growth and survival. *CPD* **10**, 191–201

10. Antunes, R. F., Brandão, C., Carvalho, G., Girão, C., and Arosa, F. A. (2009) Red blood cells carry out T cell growth and survival bioactivities that are sensitive to cyclosporine A. *Cell. Mol. Life Sci.* **66**, 3387–3398

11. Antunes, R. F., Brandão, C., Maia, M., and Arosa, F. A. (2011) Red blood cells release factors with growth and survival bioactivities for normal and leukemic T cells. *Immunol. Cell Biol.* **89**, 111–121

12. Bernard, A., Meier, C., Ward, M., Browning, T., Montgomery, A., Kasten, M., Snow, C., Manning, E., and Woodward, J. (2010) Packed red blood cells suppress T-cell proliferation through a process involving cell-cell contact. *J. Trauma* **69**, 320–329

13. Long, K., Woodward, J., Procter, L., Ward, M., Meier, C., Williams, D., and Bernard, A. (2014) *In vitro* transfusion of red blood cells results in decreased cytokine production by human T cells. *J. Trauma Acute Care Surg.* **77**, 198–201

14. Almizraq, R. J., Norris, P. J., Inglis, H., Menocha, S., Wirtz, M. R., Juffermans, N., Pandey, S., Spinella, P. C., Acker, J. P., and Muszynski, J. A. (2018) Blood manufacturing methods affect red blood cell product characteristics and immunomodulatory activity. *Blood Adv.* **2**, 2296–2306

15. Ferraris, V. A., Ballert, E. Q., and Mahan, A. (2013) The relationship between intraoperative blood transfusion and postoperative systemic inflammatory response syndrome. *Am. J. Surg.* **205**, 457–465

16. Menocha, S., and Muszynski, J. A. (2019) Transfusion-related immune modulation: Functional consequence of extracellular vesicles? *Transfusion* **59**, 3553–3555

17. Belizaire, R. M., Prakash, P. S., Richter, J. R., Robinson, B. R., Edwards, M. J., Caldwell, C. C., Lentsch, A. B., and Pritts, T. A. (2012) Microparticles from stored red blood cells activate neutrophils and cause lung injury after hemorrhage and resuscitation. *J. Am. Coll. Surg.* **214**, 648–655. discussion 656-657

18. Danesh, A., Inglis, H. C., Jackman, R. P., Wu, S., Deng, X., Muench, M. O., Heitman, J. W., and Norris, P. J. (2014) Exosomes from red blood cell units bind to monocytes and induce proinflammatory cytokines, boosting T-cell responses *in vitro*. *Blood* **123**, 687–696

19. Martins, R., Maier, J., Gorki, A.-D., Huber, K. V. M., Sharif, O., Starkl, P., Saluzzo, S., Quattrone, F., Gawish, R., Lakovits, K., Aichinger, M. C., Radic-Sarikas, B., Lardeau, C.-H., Hladik, A., Korosec, A., *et al.* (2016) Heme drives hemolysis-induced susceptibility to infection via disruption of phagocyte functions. *Nat. Immunol.* **17**, 1361–1372

20. Torrance, H. D., Brohi, K., Pearse, R. M., Mein, C. A., Wozniak, E., Prowle, J. R., Hinds, C. J., and O'Dwyer, M. J. (2015) Association between gene expression biomarkers of immunosuppression and blood transfusion in severely injured polytrauma patients. *Ann. Surg.* **261**, 751–759

21. Baron, D. M., Lei, C., and Berra, L. (2020) Old, older, the oldest: Red blood cell storage and the potential harm of using older red blood cell concentrates. *Curr. Opin. Anaesthesiol* **33**, 234–239

22. Francis, R. O., D'Alessandro, A., Eisenberger, A., Soffing, M., Yeh, R., Coronel, E., Sheikh, A., Rapido, F., La Carpia, F., Reisz, J. A., Gehrke, S., Nemkov, T., Thomas, T., Schwartz, J., Divgi, C., *et al.* (2020) Donor glucose-6-phosphate dehydrogenase deficiency decreases blood quality for transfusion. *J. Clin. Invest.* **130**, 2270–2285

23. D'Alessandro, A., Fu, X., Kanias, T., Reisz, J. A., Culp-Hill, R., Guo, Y., Gladwin, M. T., Page, G., Kleinman, S., Lanteri, M., Stone, M., Busch, M. P., and Zimring, J. C. (2020) Donor sex, age and ethnicity impact stored red blood cell antioxidant metabolism through mechanisms in part explained by glucose 6-phosphate dehydrogenase levels and activity. *Haematologica*. https://doi.org/10.3324/haematol.2020.246603

24. Gerner, M. C., Ziegler, L. S., Schmidt, R. L. J., Krenn, M., Zimprich, F., Uyanik-Ünal, K., Konstantopoulou, V., Derdak, S., Del Favero, G., Schwarzinger, I., Boztug, K., and Schmetterer, K. G. (2020) The TGF-b/SOX4 axis and ROS-driven autophagy co-mediate CD39 expression in regulatory T-cells. *FASEB J.* **34**, 8367–8384

25. Schmetterer, K. G., Goldhahn, K., Ziegler, L. S., Gerner, M. C., Schmidt, R. L. J., Themanns, M., Zebedin-Brandl, E., Trapin, D., Leitner, J., Pickl, W. F., Steinberger, P., Schwarzinger, I., and Marculescu, R. (2019) Overexpression of PDE4A acts as checkpoint inhibitor against cAMP-mediated immunosuppression *in vitro*. *Front. Immunol.* **10**, 1790

26. Schmidt, R. L. J., Jutz, S., Goldhahn, K., Witzeneder, N., Gerner, M. C., Trapin, D., Greiner, G., Hoermann, G., Steiner, G., Pickl, W. F., Burgmann, H., Steinberger, P., Ratzinger, F., and Schmetterer, K. G. (2017) Chloroquine inhibits human CD4+ T-cell activation by AP-1 signaling modulation. *Sci. Rep.* **7**, 42191

27. Ziegler, L. S., Gerner, M. C., Schmidt, R. L. J., Trapin, D., Steinberger, P., Pickl, W. F., Sillaber, C., Egger, G., Schwarzinger, I., and Schmetterer, K. G. (2021) Attenuation of canonical NF-κB signaling maintains function and stability of human Treg. *FEBS J.* **288**, 640–662

28. Wang, R., Dillon, C. P., Shi, L. Z., Milasta, S., Carter, R., Finkelstein, D., McCormick, L. L., Fitzgerald, P., Chi, H., Munger, J., and Green, D. R. (2011) The transcription factor Myc controls metabolic reprogramming upon T lymphocyte activation. *Immunity* **35**, 871–882

29. Roumenina, L. T., Rayes, J., Lacroix-Desmazes, S., and Dimitrov, J. D. (2016) Heme: Modulator of plasma systems in hemolytic diseases. *Trends Mol. Med.* **22**, 200–213

30. Boussiotis, V. A., Freeman, G. J., Taylor, P. A., Berezovskaya, A., Grass, I., Blazar, B. R., and Nadler, L. M. (2000) p27kip1 functions as an anergy factor inhibiting interleukin 2 transcription and clonal expansion of alloreactive human and mouse helper T lymphocytes. *Nat. Med.* **6**, 290–297

31. Sena, L. A., Li, S., Jairaman, A., Prakriya, M., Ezponda, T., Hildeman, D. A., Wang, C.-R., Schumacker, P. T., Licht, J. D., Perlman, H., Bryce, P. J., and Chandel, N. S. (2013) Mitochondria are required for antigen-specific T cell activation through reactive oxygen species signaling. *Immunity* **38**, 225–236

32. Minetti, M., and Malorni, W. (2006) Redox control of red blood cell biology: The red blood cell as a target and source of prooxidant species. *Antioxid. Redox Signal.* **8**, 1165–1169

33. D'Alessandro, A., Righetti, P. G., and Zolla, L. (2010) The red blood cell proteome and interactome: An update. *J. Proteome Res.* **9**, 144–163

34. Mendonça, R., Silveira, A. A. A., and Conran, N. (2016) Red cell DAMPs and inflammation. *Inflamm. Res.* **65**, 665–678

35. Bienert, G. P., Schjoerring, J. K., and Jahn, T. P. (2006) Membrane transport of hydrogen peroxide. *Biochim. Biophys. Acta* **1758**, 994–1003

36. Almasalmeh, A., Krenc, D., Wu, B., and Beitz, E. (2014) Structural determinants of the hydrogen peroxide permeability of aquaporins. *FEBS J.* **281**, 647–656

37. Moon, C., Rousseau, R., Soria, J.-C., Hoque, M. O., Lee, J., Jang, S. J., Trink, B., Sidransky, D., and Mao, L. (2004) Aquaporin expression in human lymphocytes and dendritic cells. *Am. J. Hematol.* **75**, 128–133

38. Ogura, Y., and Yamazaki, I. (1983) Steady-state kinetics of the catalase reaction in the presence of cyanide. *J. Biochem.* **94**, 403–408

39. Closa, D., and Folch-Puy, E. (2004) Oxygen free radicals and the systemic inflammatory response. *IUBMB Life* **56**, 185–191

40. Prosenz, J., Öhlinger, T., Müllner, E. W., Marculescu, R., Gerner, C., Salzer, U., Kiefer, F. W., and Baron, D. M. (2019) Glycated hemoglobin concentrations of red blood cells minimally increase during storage under standard blood banking conditions. *Transfusion* **59**, 454–457

41. Asquith, B., Debacq, C., Florins, A., Gillet, N., Sanchez-Alcaraz, T., Mosley, A., and Willems, L. (2006) Quantifying lymphocyte kinetics *in vivo* using carboxyfluorescein diacetate succinimidyl ester (CFSE). *Proc. Biol. Sci.* **273**, 1165–1171

42. Wiśniewski, J. R., Zougman, A., Nagaraj, N., and Mann, M. (2009) Universal sample preparation method for proteome analysis. *Nat. Methods* **6**, 359–362

43. Bileck, A., Kreutz, D., Muqaku, B., Slany, A., and Gerner, C. (2014) Comprehensive assessment of proteins regulated by dexamethasone reveals novel effects in primary human peripheral blood mononuclear cells. *J. Proteome Res.* **13**, 5989–6000

44. Groessl, M., Slany, A., Bileck, A., Gloessmann, K., Kreutz, D., Jaeger, W., Pfeiler, G., and Gerner, C. (2014) Proteome profiling of breast cancer biopsies reveals a wound healing signature of cancer-associated fibroblasts. *J. Proteome Res.* **13**, 4773–4782

45. Cox, J., and Mann, M. (2008) MaxQuant enables high peptide identification rates, individualized p.p.b.-range mass accuracies and proteome-wide protein quantification. *Nat. Biotechnol.* **26**, 1367–1372

46. Cox, J., and Mann, M. (2012) 1D and 2D annotation enrichment: A statistical method integrating quantitative proteomics with complementary high-throughput data. *BMC Bioinformatics* **13 Suppl 16**, S12

47. Babicki, S., Arndt, D., Marcu, A., Liang, Y., Grant, J. R., Maciejewski, A., and Wishart, D. S. (2016) Heatmapper: Web-enabled heat mapping for all. *Nucleic Acids Res.* **44**, W147–W153

48. Humphrey, S. J., Karayel, O., James, D. E., and Mann, M. (2018) High-throughput and high-sensitivity phosphoproteomics with the EasyPhos platform. *Nat. Protoc.* **13**, 1897–1916

49. Seiser, S., Janker, L., Zila, N., Mildner, M., Rakita, A., Matiasek, J., Bileck, A., Gerner, C., Paulitschke, V., and Elbe-Bürger, A. (2021) Octenidine-based hydrogel shows anti-inflammatory and protease-inhibitory capacities in wounded human skin. *Sci. Rep.* **11**, 32

50. Casado, P., Rodriguez-Prados, J.-C., Cosulich, S. C., Guichard, S., Vanhaesebroeck, B., Joel, S., and Cutillas, P. R. (2013) Kinase-substrate enrichment analysis provides insights into the heterogeneity of signaling pathway activation in leukemia cells. *Sci. Signal.* **6**, rs6

51. Hornbeck, P. V., Zhang, B., Murray, B., Kornhauser, J. M., Latham, V., and Skrzypek, E. (2015) PhosphoSitePlus, 2014: Mutations, PTMs and recalibrations. *Nucleic Acids Res.* **43**, D512–D520

52. Horn, H., Schoof, E. M., Kim, J., Robin, X., Miller, M. L., Diella, F., Palma, A., Cesareni, G., Jensen, L. J., and Linding, R. (2014) KinomeXplorer: An integrated platform for kinome biology studies. *Nat. Methods* **11**, 603–604

53. Metz, K. S., Deoudes, E. M., Berginski, M. E., Jimenez-Ruiz, I., Aksoy, B. A., Hammerbacher, J., Gomez, S. M., and Phanstiel, D. H. (2018) Coral: Clear and customizable visualization of human kinome data. *Cell Syst.* **7**, 347–350

54. Vizcaíno, J. A., Deutsch, E. W., Wang, R., Csordas, A., Reisinger, F., Ríos, D., Dianes, J. A., Sun, Z., Farrah, T., Bandeira, N., Binz, P.-A., Xenarios, I., Eisenacher, M., Mayer, G., Gatto, L., *et al.* (2014) ProteomeXchange provides globally coordinated proteomics data submission and dissemination. *Nat. Biotechnol.* **32**, 223–226

55. Baker, P. R., and Chalkley, R. J. (2014) MS-viewer: A web-based spectral viewer for proteomics results. *Mol. Cell Proteomics* **13**, 1392–1396